



Correspondence

Development of new age hardenable Mg-Li-Sc alloys



A B S T R A C T

Keywords:

MgLiSc alloys
Electron microscopy
Aged hardening
Mg-Li-Sc phase diagram

The effect of scandium addition on phase composition, precipitation hardening and mechanical properties were studied in newly designed Mg₉Li₃Sc and Mg₉Li₆Sc (wt.%) magnesium alloys. Microstructures analyzed directly after hot rolling indicated existence of α (hcp) and β (bcc) solid solutions, while after supersaturation from 470 °C and 520 °C they revealed only β (bcc) grains with MgSc particles. Following ageing at 160 and 200 °C caused hardness increase for alloys of lower and higher Sc content up to 83 HV and 93 HV, respectively. The α (hcp) Mg solid solution and MgSc particles were identified as phases responsible for their hardening. EDS analysis indicated increased scandium content within precipitates which contributed to high level of stress at α (hcp)/ β (bcc) interface manifested by high dislocation density, particularly within α phase. Thermodynamic descriptions of different phases of constituent binary alloys were extrapolated to ternary Mg-Li-Sc system using CALPHAD method. First approximation of ternary phase diagram was calculated and confronted with experimental data in Mg-rich corner of Mg-Li-Sc system. It was found that predicted phase diagram reasonably agreed with experimental evidence.

© 2018 Elsevier B.V. All rights reserved.

1. Introduction

Magnesium alloys has attracted wide attention due to their low density and a high strength suitable for structural applications [1–3]. The most popular Mg-Al-Zn alloys have been widely commercialized mainly due to their good castability [4,5]. The addition of rare earth elements (RE) to Mg alloys is very effective in enhancing their strength and high yield stress (YS) by precipitation hardening, which allows obtaining YS about 200 MPa [5]. Recently, high-strength Mg alloys, particularly Mg-Y-Zn based on YS \approx 270 MPa with a long-period stacking ordered (LPSO) phase have been developed [6] and some with Sn addition attain UTS above 400 MPa [7]. However, the Mg alloys with the hexagonal close-packed (hcp) structure tend to show low ductility at room temperature. To improve formability of α (hcp) Mg alloys, intense research over the last years has been carried out [5–8]. The improvement of plasticity was reported in Refs. [5,9] by the introduction of a body-centered cubic structure β (bcc) to the magnesium alloys by the lithium addition. Two-phase α (hcp) + β (bcc) alloys are particularly interesting, showing good mechanical properties like strength and ductility after extrusion and subsequent Equal Channel Angular Pressing (ECAP). They reveal excellent superplastic properties with the maximum elongation of about 970% at 200 °C [9]. Third additions to Mg-Li alloys often improve mechanical properties as in the two-phase Mg₈Li₂Zn (in wt.%) alloy manifesting good superplastic properties at elevated temperatures in the extruded and rolled state [10,11]. The superplastic deformation was also observed in the ultrafine-grain Mg₉Li₁Zn alloy [12] in the temperature range between 200 and 300 °C in which the diffusion controlled grain boundary sliding was visible. The addition of aluminum to the

Mg₁₅Li alloy improved its strength, which was attributed to the precipitation of Al-Li intermetallic compounds in the β -phase and grain size refinement [13]. Ternary Mg-Li-Al alloys show also good superplastic properties. The best results were obtained for the Mg₉Li₁Al alloy at 300 °C [14], as in Ref. [12], where the improvement of superplastic properties was observed after equal channel angular extrusion.

There are a few papers published recently, on the ternary Mg-Li-Sc alloys from the α (hcp), α (hcp)+ β (bcc) and β (bcc) ranges [15–19]. The rolled and annealed Mg₃Li and Mg₃Li₁Sc (wt.%) alloys were investigated in Ref. [15]. The results showed that the Sc addition refined the microstructure of the Mg₃Li alloy through the increase of the recrystallization temperature by more than 100C. Both, the strength and ductility improved significantly with the addition of Sc due to the precipitation of MgSc cubic particles and grain refinement [15]. Studies of mechanical properties of Mg-Sc alloys containing up to 0.7 wt.% Sc indicated that the solid solution strengthening effect of hexagonal Mg-Sc was low compared with other Mg-RE alloys due to the limited ability of Sc to act as an obstacle for dislocations and twin boundaries [16]. The results suggested that the small atomic misfit and the reduction of SFE (stacking fault energy) due to the Sc additions were decisive factors in the determination of the mechanical behavior of the alloys. The Mg-Sc alloy with the β single-phase showed the tensile strength of 254 MPa and elongation of 25.4%. The tensile strength of the Mg-Sc alloy increased with growing volume fraction of the α phase and the alloy showed high ultimate tensile strength (UTS) of 310 MPa and elongation of 28.8%, the properties which were better balanced than those of conventional Mg alloys. Moreover, the β -type Mg_{16.8}Sc (at.%) alloy showed age hardening at 200 °C due to the

formation of fine hcp α (hcp) needles and/or plates in the β (bcc) matrix. It also exhibited high hardness near 100 HV in the (α (hcp) + β (bcc)) Mg-Sc alloys [18], however much higher hardness approaching 230 HV was observed in the earlier work of these authors on aged β (bcc) alloys [19], in which the precipitation of the hexagonal α (hcp) phase was responsible for such a hardness increase. This result seems to be too high and was not confirmed in other investigations. Recently, Ogawa et al. [3] claimed that the Mg alloy with additions of 13–30 at.% Sc revealed superplastic effect in the association with stress-induced transformation involving the bcc phase and shape memory effect (due to a reversible martensitic transformation between the α (hcp) parent phase and the orthorhombic martensite phase).

In the literature there is no information concerning the phase relations in the Li-Mg-Sc alloys since this ternary system has not been experimentally studied yet. The only thermodynamically assessed phase diagrams refer to the binary Li-Mg [20], Li-Sc [21], Mg-Sc [22,23] ones. The Li-Mg [20] system consists of three phases: liquid, α (hcp) Mg and β (bcc) Li solid solutions. Lithium dissolves in the Mg α (hcp) phase up to 6 wt.%, whereas the solubility of Mg in the Li β (bcc) phase is close to 90 wt.%. The β (bcc) phase containing the highest Mg content melts at 590 °C. In contrast to Mg-Li, in the Li-Sc system the solubility of Sc in the Li-based (β)bcc phase, as well as the solubility of Li in the (α)hcp and (β)bcc Sc are practically nonexistent [21]. It should be noted that Bu et al. [21] based their work on the phase diagram constructed by Okamoto [24] with very limited data [25], and it needs experimental confirmation. The Mg-Sc phase diagram reassessed by Kang et al. [23] was very similar to the earlier assessment of Pisch et al. [22]. One distinct difference concerned the MgSc phase which was modeled as nonstoichiometric (bcc_B2 solid solution) in Ref. [23], whereas Pisch et al. modeled it as a linear compound [22] due to insufficient experimental data. The solubility of Sc in the (α)hcp Mg phase reaches 33 wt.% at 480 °C. The Sc-based (β)bcc solid solution contains up to 68 wt.% of Mg at 710 °C. Because of missing experimental evidence the Sc-rich part of Mg-Sc phase diagram has been considered tentative [22,23].

A new alloy was developed in the study assuming the existence of similar phase composition in the Mg-Li [4] and Mg-Sc [14] alloys, namely α (hcp) and β (bcc) showing good plasticity and strength, particularly at room temperature (RT) [7–14]. Due to lack of information on the ternary Mg-Li-Sc phase diagram it was approximated using the extrapolation of CALPHAD descriptions of binary systems into the ternary one. The effect of scandium addition on the phase composition, deformation ability and mechanical properties due to precipitation hardening was studied in new alloys based on Mg9Li with additions of 3–6 wt.% of Sc revealing also α (hcp) + β (bcc) structures.

2. Experimental procedure

2.1. Sample preparation

The ternary Mg-Li-Sc alloys: (91-x)Mg(9)Li(x)Sc where $x = 3$ wt.% (designated as Mg9Li3Sc) and 6 wt.% (designated as Mg9Li6Sc) were prepared from pure components: Mg (99.99 wt.%), Li (99.9 wt.%), Sc (99.97 wt.%). Because the alloy components greatly differed with respect to melting temperature (Li 180.5 °C, Sc 1541 °C), the preparation of alloys was divided into steps. First, Mg10Sc (wt.%) base alloy was prepared by induction melting, next, it was added to Li and Mg in such proportions that gave the desired Sc content in the final ternary alloy. Because liquid Li readily reacts with graphite and many ceramics, the ternary alloys were prepared in a molybdenum crucible. The resistance furnace was closed in a glovebox filled with high purity argon gas

(99.9997%) circulating in a closed circuit and additionally purified with Ti-shavings at 850 °C. At this temperature Ti reacted with traces of oxygen, moisture and nitrogen, removing them from the glovebox. The crucible with alloy components was put into the furnace already heated to 800 °C. Once its content was liquid, it was stirred carefully and cast into steel mold of rectangular cross-section. The mass loss of such prepared alloys was below 0.5%. The castings were removed from molds, let to cool freely and then put into another furnace already preheated to 400 °C for 5 h to promote homogenization. Both alloys were hot rolled at 350 °C up to the thickness reduction of 70% using the quarto-duo DW4-L rolling mill. The deformation temperature was chosen as low as possible to allow deformation of the cast sample and to avoid the dynamic grain growth assuming that scandium increases the recrystallization temperature as was observed in the Mg-Sc and Mg-Li-Sc alloys [4,14–16]. The hot rolled samples were solutionized at 470 °C and 520 °C for 1.5 h, next aged at 160 °C and 200 °C for 0.15–120 h. To avoid oxidation effect the samples were closed in a quartz tube in which the vacuum was applied.

2.2. Microstructure and mechanical properties

The samples for the structural characterization were taken both from the longitudinal direction of the ingot and after the deformation. The microstructural observations were performed using a Leica optical microscope in Nomarski interference contrast with the QUIN image analysis system. The bright-field (BF) microstructure and selected area electron diffraction pattern (SADP) studies were carried out using Tecnai G2 F20 and Philips CM20 transmission electron microscopes (TEM) with the integrated Energy-Dispersive X-ray Spectroscopy system (EDS). Thin samples of hot pressed alloys were cut with electro spark, then dimpled and electropolished in the electrolyte consisting of 750 ml AR grade methanol, 150 ml butoxyethanol, 16.74 g magnesium perchlorate and 7.95 g lithium chloride and finally dimpled using Gatan dimpler and ion beam thinned using Leica EM RES101 ion beam thinner. The hardness of samples was tested with a Zwick ZHU 250 instrument using the Vickers method under 50 N of load (HV5) and the tensile tests were performed at Instron 6025 testing machine at room temperature.

3. Results and discussion

3.1. Prediction of Mg-Li-Sc phase diagram with binary approximation method

A common approach in calculating ternary phase diagrams is to start from the extrapolation of CALPHAD descriptions of binary systems into the ternary one [26]. This gives reasonably good results when a proper extrapolation scheme is used for terminal solution phases i.e. extending from pure components. All of the liquid and solid solution phases in the Mg-Li, Li-Sc and Mg-Sc systems were described with regular or sub-regular solution model (with exception of liquid in Ref. [23]). The Modified Quasichemical Model (MQM) used for the liquid phase of Mg-Sc in Ref. [23] is much different from the models used for the liquid phase of Mg-Li and Li-Sc [20,21], therefore in the first approximation of Li-Mg-Sc phase diagram an earlier assessment of Mg-Sc system [22] was adopted. The ternary Li-Mg-Sc phase diagram was extrapolated from the binary systems provided that the phases with the same crystallographic structure have the same models, therefore their behavior in the ternary one can be predicted.

The liquid, ((β)Li and (β)Sc) (β)bcc, ((α)Mg and (α)Sc) (α)hcp were modeled as disordered solutions. The Gibbs energies G° for

the ternary solution phases \emptyset are obtained by extrapolating the binary energies using formula (1):

$$G^{\emptyset} = x_1 {}^0G_1^{\emptyset} + x_2 {}^0G_2^{\emptyset} + x_3 {}^0G_3^{\emptyset} + RT[x_1 \ln(x_1) + x_2 \ln(x_2) + x_3 \ln(x_3)] + x_1 x_2 \sum_i L_{12}^i (x_1 - x_2)^i + x_1 x_3 \sum_i L_{13}^i (x_1 - x_3)^i + x_2 x_3 \sum_i L_{23}^i (x_2 - x_3)^i. \quad (1)$$

Where: x_1, x_2, x_3 are mole fractions of components 1,2,3; ${}^0G_1^{\emptyset}, {}^0G_2^{\emptyset}, {}^0G_3^{\emptyset}$ are Gibbs energies of reference states of elements 1, 2, 3 as taken from SGTE pure elements database; $L_{12}^i, L_{13}^i, L_{23}^i$ are coefficients of excess Gibbs energy terms, which have the same value as for binary systems listed in Table 1, R is universal gas constant, T is absolute temperature.

Gibbs energy of stoichiometric MgSc phase [22], referenced to Mg and (α)Sc, is expressed by equation (2), where $\Delta_f G$ is Gibbs energy of formation of MgSc phase.

$$G^{MgSc} = 0.5 {}^0G_{Mg} + 0.5 {}^0G_{Sc} + \Delta_f G \quad (2)$$

3.2. Analysis of predicted Mg-Li-Sc phase diagram

Fig. 1 illustrates the calculated liquidus projection in the Mg-rich corner of Mg-Li-Sc system. The calculated liquidus temperature of the experimentally investigated alloys, marked as points (x) in Fig. 1, is in the range of 600–610 °C and the (β)bcc solid solution is a primary solidification phase. As illustrated in Fig. 2, two alloys investigated should have different phase composition at 400 °C. The alloy with 6 wt.% Sc should be composed of two phases in the equilibrium: (β)bcc and intermetallic MgSc. The alloy containing 3 wt.% Sc should be the single (β)bcc phase. Fig. 3 shows the change of phase composition of the Mg9Li alloy with the scandium addition. What is interesting, the solubility of scandium in the (β) bcc phase increases with temperature and above 430 °C only bcc solid solution in the alloy containing 6 wt.% Sc should exist. Another important feature is that the (α)hcp and MgSc phases should precipitate from the quenched alloy, therefore one should expect age hardening of the Mg9Li (wt.%) alloy with scandium addition.

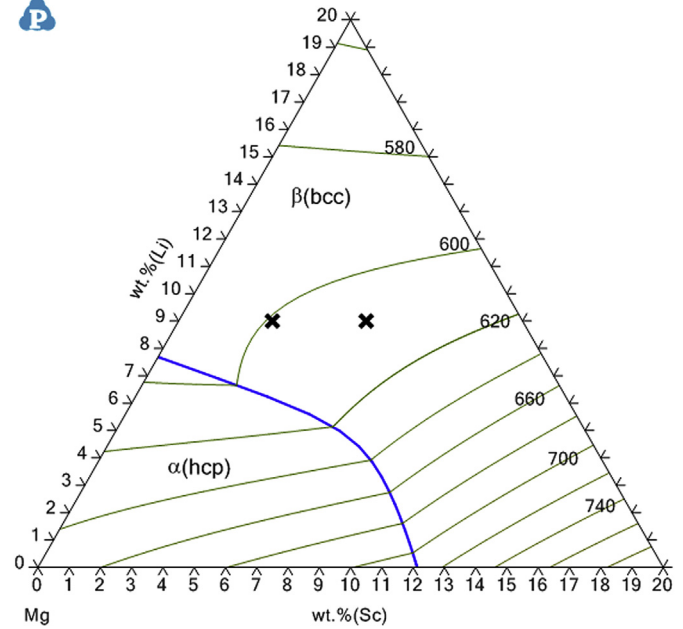


Fig. 1. Predicted liquidus projection in the Mg-rich corner of Mg-Li-Sc system. Isotherms in °C; points (x) correspond to compositions of investigated alloys Mg9Li3Sc and Mg9Li6Sc.

3.3. Effect of hot rolling

Table 2 shows the results of hardness measurements and tensile test of hot rolled Mg9Li3Sc and Mg9Li6Sc alloys. It can be seen that the hardness of the Mg9Li6Sc alloy is slightly higher than that of Mg9Li3Sc. The hardness is higher than that of the deformed two phase Mg9Li1.5Al alloy [27], which indicates a positive effect of scandium on the mechanical properties of Mg-Li system in agreement with the results of earlier studies [15–17]. The observed tensile strength is also much higher than that of rolled Mg9Li alloy where the maximum strength of 135 MPa was reported [28]. High compression strength near 250 MPa reported in Ref. [6] in the Mg-Li-Al alloys with 3–5 wt.% Al was accompanied by a low ductility and could not be directly compared with tensile strength of the investigated alloys. Fig. 4 shows optical images taken of the

Table 1
Thermodynamic parameters of binary Mg-Li, Li-Sc and Mg-Sc systems [20–22].

Phase	System	Parameters	Reference	
Liquid	Li-Mg	$L_{LiMg}^0 = -14935 + 10.371T$	[20]	
		$L_{LiMg}^1 = -1789 + 1.143T$		
	Li-Sc	$L_{LiMg}^2 = 6533 - 6.6915T$	[21]	
		$L_{LiSc}^0 = 15519$		
β (bcc)	Mg-Sc	$L_{LiSc}^1 = 7913$	[22]	
		$L_{LiSc}^2 = -5283$		
	Li-Mg	$L_{MgSc}^0 = -12000 + 8.75T$	[20]	
		$L_{LiMg}^0 = -18335 + 8.49T$		
		Li-Sc	$L_{LiMg}^1 = 3481$	[21]
			$L_{LiMg}^2 = 2658 - 0.114T$	
α (hcp)	Mg-Sc	$L_{LiSc}^0 = 47776$	[21]	
		$L_{LiSc}^1 = -14574$		
	Li-Mg	$L_{MgSc}^0 = -24051 + 15.56T$	[22]	
		$L_{LiMg}^0 = -6856$		
		Li-Sc	$L_{LiMg}^1 = 4000$	[20]
			$L_{LiMg}^2 = 4000$	
MgSc	Li-Sc	$L_{LiSc}^0 = 58238$	[21]	
	Mg-Sc	$L_{MgSc}^0 = -16115.8 + 15.02T$	[22]	
	Mg-Sc	$G^{MgSc} = 0.5 {}^0G_{Mg} - 0.5 {}^0G_{Sc} = -21926T + 2T + 2.694T \ln T$	[22]	

P
400 °C

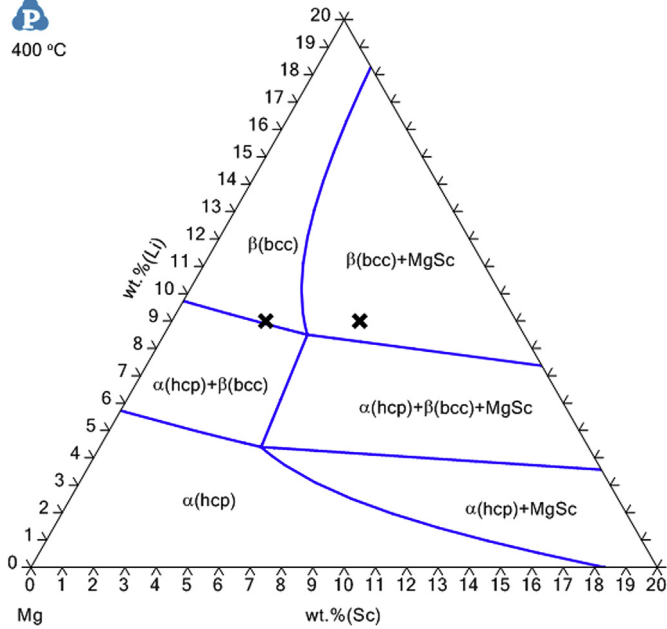


Fig. 2. Predicted isothermal section at 400 °C in the Mg-rich corner of Li-Mg-Sc system. Points (x) correspond to compositions of investigated alloys Mg9Li3Sc and Mg9Li6Sc.

Mg9Li3Sc and Mg9Li6Sc hot rolled alloys at 350 °C. Micrograph 4a taken of the Mg9Li3Sc alloy shows two-phases elongated in the rolling direction, probably $\alpha(\text{hcp})$ visible as bright and $\beta(\text{bcc})$ giving gray contrast (matrix) in accordance with the phase diagram prediction in Fig. 2. Within the darker $\beta(\text{bcc})$ phase some finer black particles can be seen which can be MgSc precipitates. Fig. 4b shows a different microstructure with finer grains of $\alpha(\text{hcp})$ and $\beta(\text{bcc})$ showing less pronounced directionality and fine dark precipitates, most probably MgSc (≈ 4 vol%), identified using EDS as Sc enriched,

Table 2

Hardness and tensile test results of investigated hot rolled alloys Mg9Li3Sc and Mg9Li6Sc.

Rolled alloys	Hardness HV ₅	UTS [MPa]	$\sigma_{0.2}$ [MPa]	Elongation %
Mg9Li3Sc	63 ± 1	173	62	45
Mg9Li6Sc	66 ± 2	184	77	30

which is consistent with the phase diagram in Fig. 2. These observations indicate that the extrapolation of phase diagram from the binary systems (Fig. 2) reasonably predicts phases existing above 300 °C. XRD patterns for samples after rolling are shown in Fig. 4c. These results confirm presence of $\alpha(\text{hcp}) + \beta(\text{bcc})$ with a small amount of MgSc precipitations. Higher volume of $\alpha(\text{hcp})$ phase is observed in Mg9Li3Sc alloy, what indicates that Sc stabilizes $\beta(\text{bcc})$ structure in Mg-Li-Sc system.

Fig. 5 shows a TEM micrograph from the Mg9Li3Sc sample after hot rolling. The subgrain boundary between the bright and dark grain of the $\beta(\text{bcc})$ phase can be seen together with dark precipitates within the $\beta(\text{bcc})$ phase. The selected area diffraction pattern (SADP) from the upper darker grain shows the [001] zone axis orientation of the $\beta(\text{bcc})$, and additional weak reflections that can be indexed as the $\alpha(\text{hcp})$ at the [0001] zone axis orientation. The $\alpha(\text{hcp})$ precipitates are visible in Fig. 5b as bright in the DF micrograph taken using $10\bar{1}0$ $\alpha(\text{hcp})$ phase reflection. They were formed most probably during the high temperature treatment before the plastic deformation (annealing) and during hot rolling below 350 °C. Low dislocation density indicated to a partial recovery at that deformation temperature.

Fig. 6 shows TEM micrographs of the Mg9Li6Sc after hot rolling taken in the bright and dark field using $01\bar{1}0$ $\alpha(\text{hcp})$ reflection. One can see that particles of the $\alpha(\text{hcp})$ phase (marked with arrow) are of lamellar form as observed also in Mg-Li-Al alloys [3–8,17] of the $\alpha(\text{hcp}) + \beta(\text{bcc})$ structure. These areas are rather small and were not observed after quenching due to the stabilization of the $\beta(\text{bcc})$ phase with scandium addition. The α phase appeared most

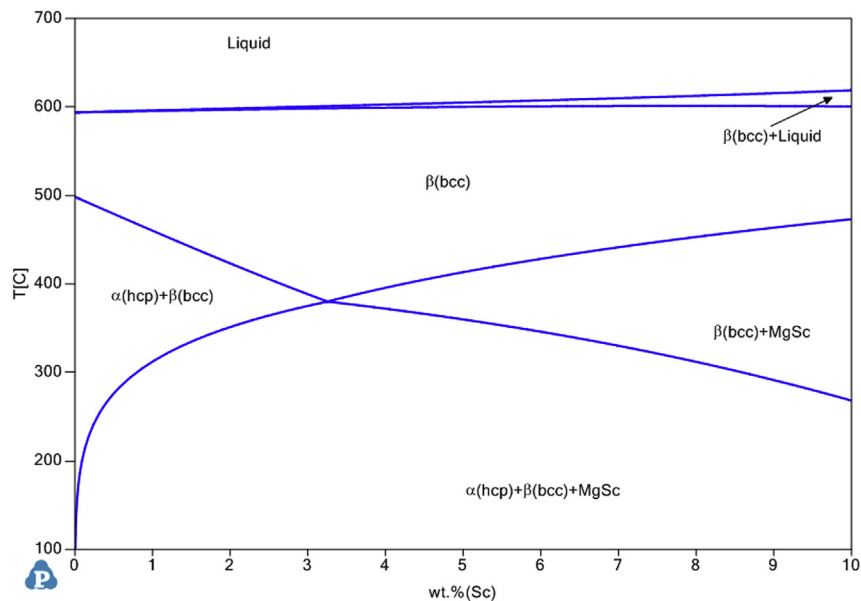


Fig. 3

Fig. 3. Predicted iso-pleth in the Li-Mg-Sc system at fixed Li concentration (Li: 9 wt%).

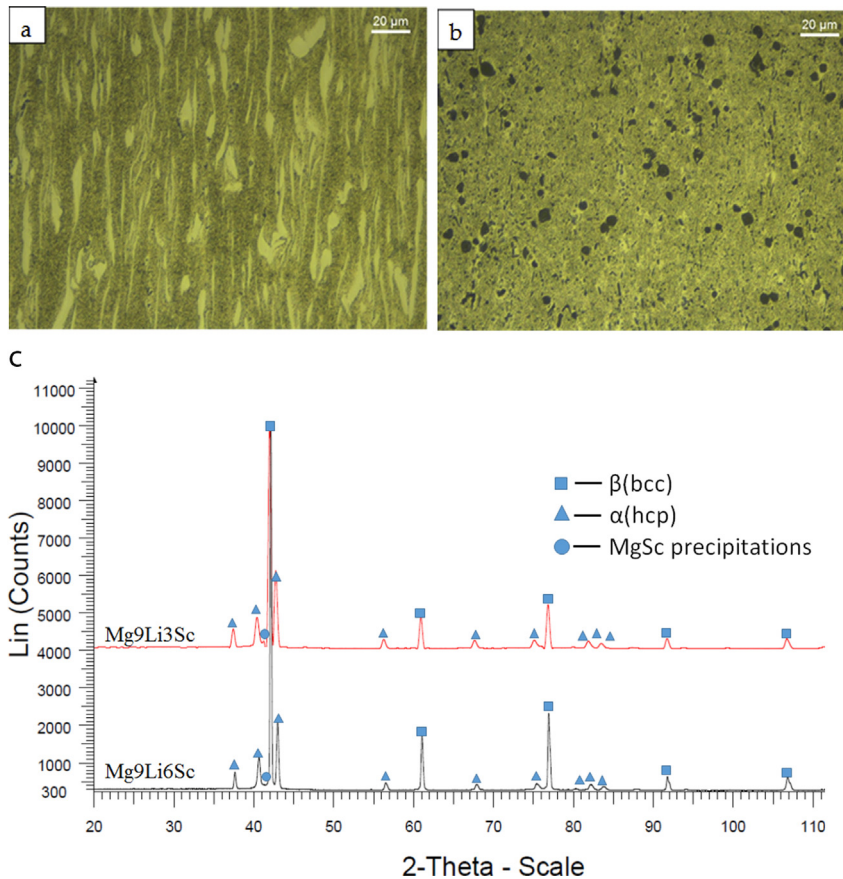


Fig. 4. Optical microstructures of alloys after rolling up to 70% of deformation at 300 °C; a) Mg9Li3Sc, b) Mg9Li6Sc, c) XRD patterns for both alloys.

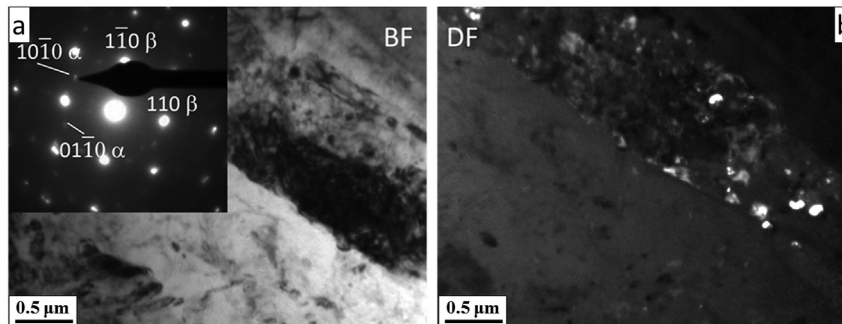


Fig. 5. Alloy Mg9Li3Sc after rolling up to 70% of reduction at 300 °C; a) BF micrograph and selected area diffraction pattern SADP as an insert, DF image taken using $10\bar{1}0$ reflection of the α (hcp) phase (b).

probably after heating and deformation since the alloys of composition near equilibrium of both phases are unstable and the precipitates of α (hcp) phase were often observed within the β (bcc) one [8]. The TEM micrograph on the left side of Fig. 7 contains a large particle with a clear pattern of perpendicular lines. Such particles are visible in the optical micrograph in Fig. 4b and also in the as-quenched samples in Fig. 8. The SADP from this particle shown as an insert in Fig. 7 can be indexed as [001] zone axis orientation of the ordered MgSc phase and the parallel lines most probably indicate ordered domain walls. The presence of MgSc phase at this composition range was predicted in the calculated Mg-Li-Sc phase diagram in Fig. 2; however it should disappear above 430 °C even in the Mg9Li6Sc alloy as results from Fig. 3. Therefore considering the experimental results, the line separating the regions of β (bcc) and

β (bcc) + MgSc in Fig. 3 should be shifted most probably to higher temperatures.

3.4. Age hardening of Mg-Li-Sc

Fig. 8 shows the optical microstructures of Mg9Li3Sc (a) and Mg9Li6Sc (b) alloys quenched from 520 °C into water. Significant changes in the morphology in relation to hot rolled state are visible. The structure changes after quenching correspond to near single β (bcc) phase and the increased average grain size up to 170 μm and 75 μm for the Mg9Li3Sc and Mg9Li6Sc alloys, respectively. It results probably from the recrystallization followed by coarsening effect occurring during supersaturation at 520 °C. Additionally, bands of dark particles in the amount of ≈ 3 and 5 vol.%, respectively for

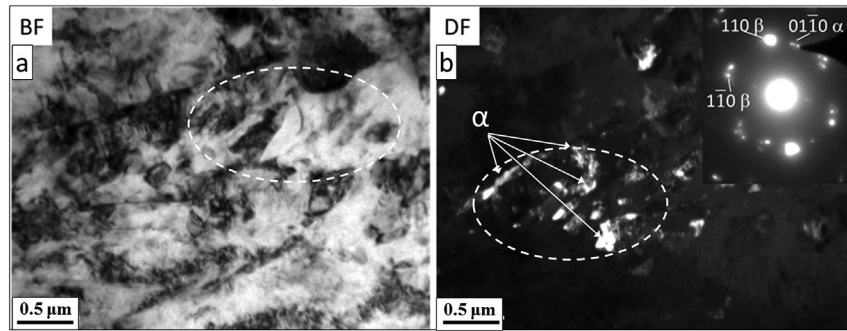


Fig. 6. a) TEM bright field and, b) dark field micrographs of Mg9Li6Sc alloy rolled at 300 °C up to 70% reduction. SADP included as insert in DF image shows reflections from β phase at $[111]$ zone axis orientation and from α (hcp) phase at $[10\bar{1}0]$ zone axis orientation. DF taken using $01\bar{1}0$ α reflection marked in SADP. Arrows indicate α -phase particles visible as bright in the DF micrograph within the β elliptical area highlighted in Fig. 6a and b.

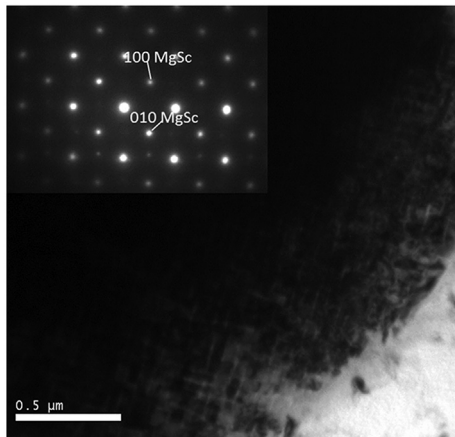


Fig. 7. TEM micrograph of Mg9Li6Sc alloy rolled at 300 °C up to 70% reduction. SADP in the upper left part from left dark grain showing MgSc intermetallic phase at $[001]$ zone axis orientation.

the Mg9Li3Sc and Mg9Li6Sc are visible in the rolling direction. The particles are likely to be MgSc phase according to the predicted phase diagram in Fig. 2 and X-ray diffraction studies shown in Fig. 8c. No α (hcp) phase can be seen there, which is in agreement with Fig. 3 where the predicted phase constitution based on thermodynamic calculations is shown. The X-ray analysis of Mg9Li3Sc after quenching (Fig. 8c) confirmed the presence of β (bcc) solid solution with small amount (below 3 vol.%) of MgSc particles.

The accuracy of ternary extrapolation from binary systems depends on the quality of assessments of the binary systems as well as probability and magnitude of ternary interactions [29]. The thermodynamic description of Li-Mg [20] and Mg-Sc [22,23] (in the Mg-rich part) was verified experimentally, while, as pointed out earlier, the assessed Li-Sc [21] phase diagram was based on a very limited experimental work. This may explain the differences between the extrapolated phase diagram (Figs. 2 and 3) and the microstructures of investigated alloys (Figs. 4–8). Several ternary Mg-alloys [30] contain ternary intermetallic compounds (stoichiometric) as well as ternary intermetallic solution phases extending

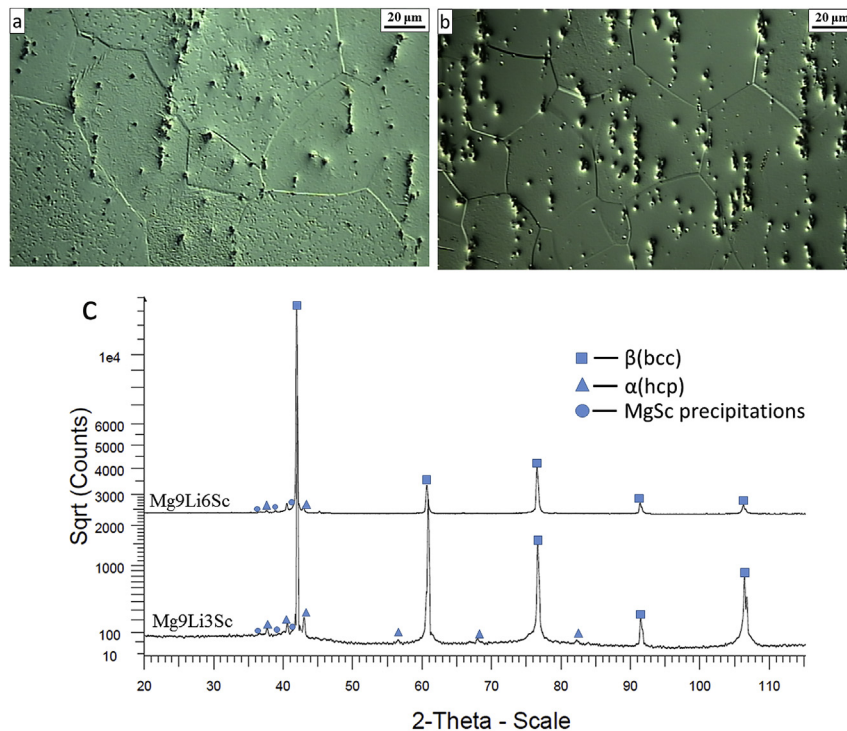


Fig. 8. Optical microstructures of rolled and quenched from 520 °C a) Mg9Li3Sc, b) Mg9Li6Sc, and c) X-ray analysis results for both alloys quenched from 520 °C.

from the binary ones. There are no intermetallic binary phases in the Mg-Li and Li-Sc systems; moreover the latter shows liquid miscibility gap. Therefore, despite there is intermetallic phase in the Mg-Sc system, it could be assumed that the probability of ternary stoichiometric phase appearance is low in the Li-Mg-Sc system. Taking the above into account and considering that the Mg-rich corner of Li-Mg-Sc ternary diagram is being focused on, in the first approximation the extrapolation directly from the existing binary descriptions seems fully justified. When the evidence of ternary interactions becomes available, the thermodynamic description of Li-Mg-Sc ternary system can be updated. The MgSc phase possesses the B2 ordered structure [23]. The solubility of MgSc is likely to change with temperature as results from isopleth in Fig. 3, therefore quenching from 520 °C to 470 °C was performed followed by ageing. Quenching from higher temperatures than 530 °C caused partial melting of the alloys, therefore the highest quenching temperature of 520 °C was applied. Next, the samples were aged at 160 °C and 200 °C and the results of hardness measurements are shown in Figs. 9 and 10, respectively for Mg9Li3Sc and Mg9Li6Sc. It can be seen that the alloys quenched from higher temperature attained higher hardness during ageing. The maximum hardness of alloy MgLi9Sc3 aged at 160 °C was 77 HV compared with 90 HV for the alloy quenched from 470 °C. The similar situation was observed for the alloys aged at 200 °C, however the highest hardness achieved during ageing was lower. The alloys containing 6 wt.% Sc also gained higher hardness after quenching from 520 °C and that accomplished during thermal treatment at 160 °C was 92 HV compared with 89 HV reached after quenching from 470 °C. The differences are not large, about 10%. Additionally, the hardness of both alloys is different after quenching and that of alloy containing 6 wt.% of Sc is higher by about 15 HV than that of the alloy with 3 wt.% of Sc. This difference is most probably caused by larger density of MgSc primary particles as well as increased volume of Sc content in the Mg solid solution. The increase of hardness after aging is connected with MgSc and α (hcp) precipitations being similar for both alloys.

The differences in hardness in as-quench state are most probably caused by higher solubility of Sc in β (bcc). However, it does not result from Fig. 3, but concerns a relatively short annealing time (1.5 h). It can be assumed that the increased solubility of Sc was attained at higher temperature, which brought about higher density of precipitates and contributed to higher hardness.

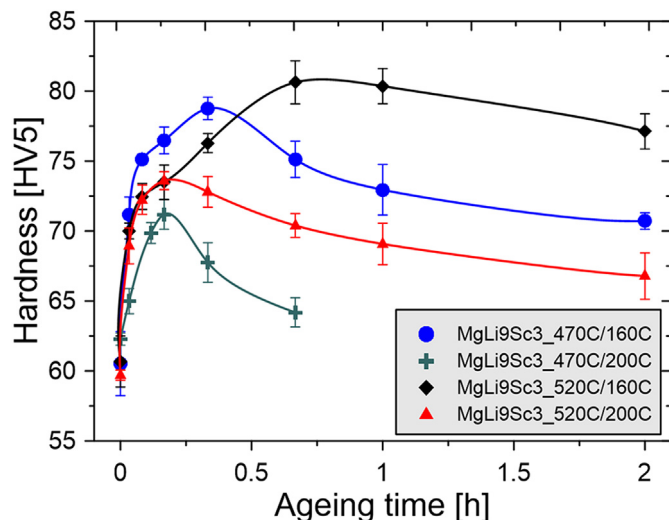


Fig. 9. Hardness versus ageing time of Mg9Li3Sc alloy saturated at 470 °C and 520 °C for 1.5 h, quenched into water and aged at 160 °C and 200 °C for 0.15–120 h.

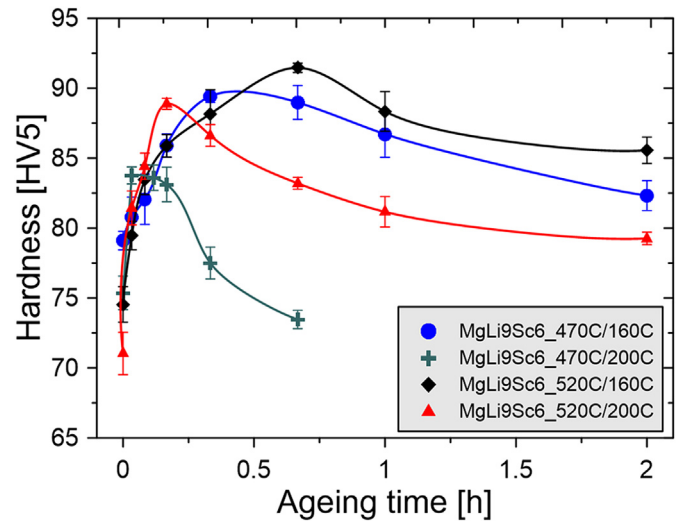


Fig. 10. Hardness versus ageing time of alloy Mg9Li6Sc saturated at 470 °C and 520 °C for 90 min, quenched into water and aged at 160 °C and 200 °C for 0.15–120 h.

The age hardening effect for the Mg9Li6Sc was rather large, since hardness increased during ageing from 74 HV to 92 HV, however the gain resulting from the increase of scandium content was not too large. The identification of the precipitating phase is therefore important. The question is, whether it is the α (hcp) phase as shown in the binary MgSc alloys [18,31].

Fig. 11 shows the results of tensile test of the Mg9Li3Sc alloy after: (i) hot rolling, (ii) quenching from 520 °C/H₂O and (iii) quenching followed by ageing at 160 °C for 40 min. It can be seen that the sample aged to the maximum hardness reached the highest strength, while the lowest hardness was obtained in the as-quenched state and the rolled sample acquired intermediate strength. All samples showed very good ductility near 40%, what is much higher than for popular magnesium based alloys [4].

There was no work hardening observed contrary to the hexagonal Mg-Sc alloys in which some hardening reported in Ref. [16] was

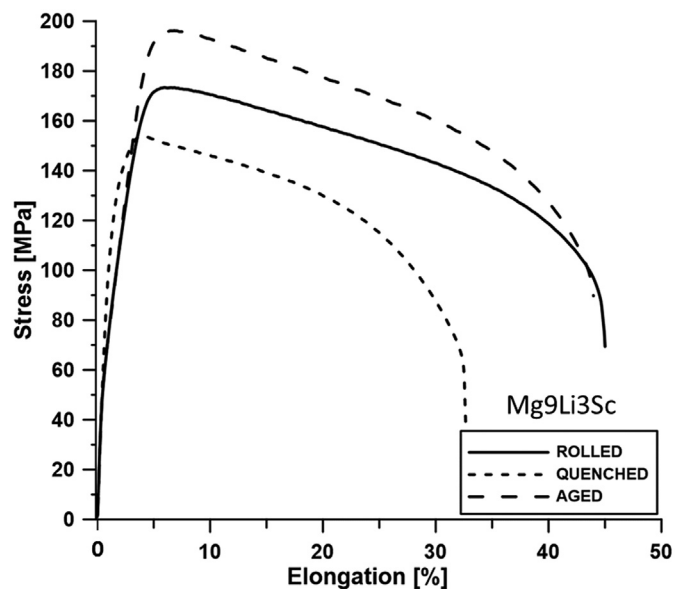


Fig. 11. Tensile curves of Mg9Li3Sc samples in as-rolled state, as-quenched (520 °C/1.5h) and quenched (520 °C/1.5h) and aged (160 °C for 40 min).

due to the low atomic misfit leading to low strengthening of slip and twinning. Similar phenomenon was observed in the $\alpha(\text{hcp}) + \beta(\text{bcc})$ and $\beta(\text{bcc})$ Mg-Sc alloys, i.e. no work hardening in the $\beta(\text{bcc})$ alloys at 20% Sc and small hardening in the $\alpha(\text{hcp}) + \beta(\text{bcc})$ state [16–18] in accord with previous studies on Mg-Sc alloys [16] in which it was shown that the Sc addition to Mg exerted a weak influence on hardening of deformation modes that determined yield stress. In addition, the $\beta(\text{bcc})$ single-phase sample showed hardly any work hardening [17–19]. It seems that the addition of scandium increased the phenomenon observed in Mg-Li-Zn $\alpha(\text{hcp}) + \beta(\text{bcc})$ alloys such as low temperature activation of $\alpha(\text{hcp})/\beta(\text{hcp})$ phase boundary sliding [11,12].

Table 3 shows the results of tensile tests of the samples cut from

Table 3

Hardness and tensile test results of investigated alloys Mg9Li3Sc and Mg9Li6Sc quenched from 520 °C, aged to maximum hardness at 160 °C.

Composition of alloy	Hardness HV _{0.05}	UTS [MPa]	$\sigma_{0.2}$ [MPa]	Elongation %
Mg9Li3Sc	81 ± 2	196	66	44
Mg9Li6Sc	92 ± 1	227	121	20

the both investigated alloys aged to the maximum hardness at 160 °C after quenching from 520 °C. One can see that UTS measured at room temperature (RT) was above 220 MPa, which was much higher than that observed for the $\alpha + \beta$ Mg-Li-Al-Zn alloys [32] and close to that reported for the $\alpha(\text{hcp}) + \beta(\text{bcc})$ Mg-Sc alloys [18]; however lower than observed in the aged β alloys [17], what is astonishing in view of the results for the $\alpha(\text{hcp}) + \beta(\text{bcc})$ alloys of higher scandium content. The ductility was also higher than that reported for the Mg-Li base alloys.

Fig. 12 shows the STEM micrograph and elemental mapping of the alloy Mg9Li6Sc aged 10 minutes at 200 °C. Large bright particles in the $\beta(\text{bcc})$ matrix with a clear contrast from fine precipitates responsible for the increase of hardness can be seen. Elemental mapping of Sc and Mg (lithium cannot be detected using the EDS detector) reveals that large precipitates are rich in scandium and depleted in magnesium, which confirms the electron diffraction identification of the MgSc phase, since the matrix contains close to 90 wt.% of Mg.

Fig. 13 contains a set of TEM micrographs and SADP taken of the Mg9Li3Sc alloy quenched from 470 °C and aged 40 minutes to the maximum hardness. The SADP shows the basic orientation of

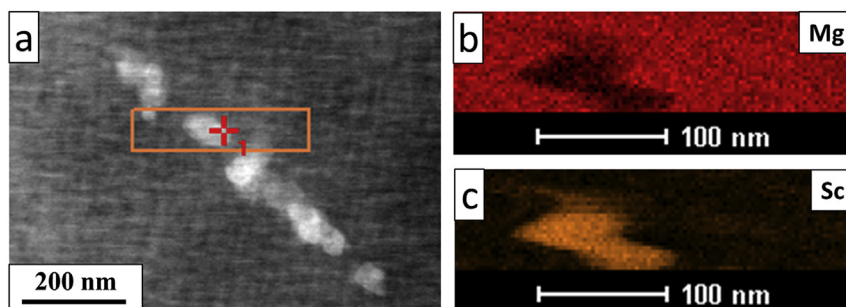


Fig. 12. a) STEM micrograph and elemental mapping distribution b) Mg, c) Sc for Mg9Li6Sc after quenching from 520 °C and aged for 10 minutes at 200 °C showing distribution of magnesium and scandium within large particle.

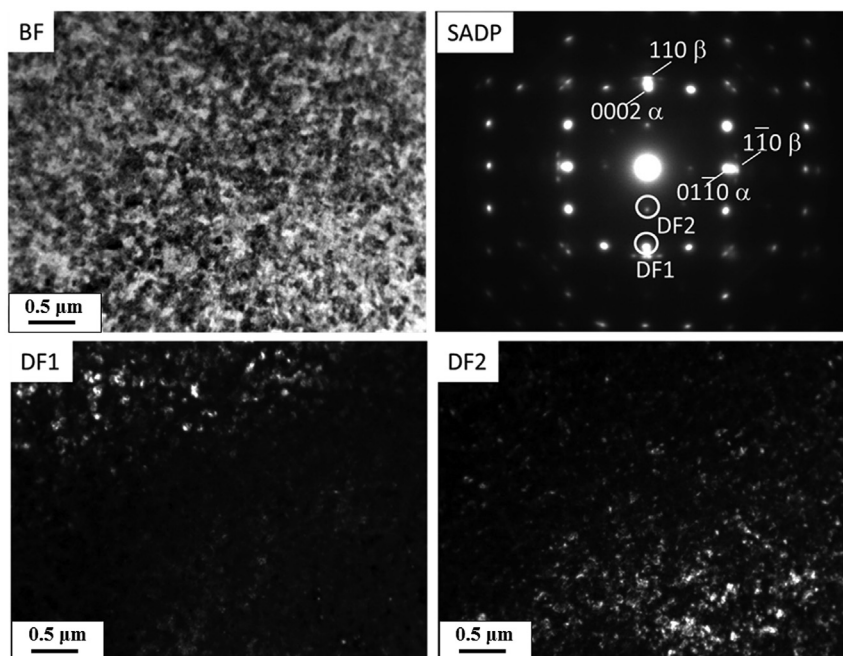


Fig. 13. TEM bright field and dark field micrographs of the alloy Mg9Li3Sc quenched from 520 °C/1.5h and aged for 40 minutes at 160 °C to maximum hardness. DF1 and DF2 were taken using various reflections of $\alpha(\text{hcp})$ phase marked in SADP.

β (bcc) phase of [011] zone axis orientation and the additional reflections at positions near $\frac{1}{2}(110)$ corresponding to 0001 α (hcp). No reflections were observed at position 100 β (bcc) what indicated that precipitates were not the MgSc phase, but it suggested the precipitation of the α phase. Dark field images (DF1 and DF2) shown in Fig. 13 were taken using 0001 and 0002 reflections of the α (hcp) phase, respectively and contained bright precipitates of size below 100 nm. The precipitation of the α (hcp) phase was observed in binary Mg-Sc alloys [18, 31], in a needle form observed already using the optical microscopy. Aging precipitation kinetics and hardening of the binary Mg-Sc alloy with β (bcc)- α (hcp) two-phase were attributed to the precipitation of very fine α (hcp) phase in the β (bcc) phase [31]. Nevertheless, the hardening effect and the time to attain maximum hardness were similar. Fine hexagonal precipitates were also observed in the binary Mg14Li β -alloys [33,34], however no hardening effect was reported. A similar microstructure can be seen in Fig. 14 (BF) taken of the Mg9Li6Sc alloy aged at 200 °C to the maximum hardness. The high density of precipitates can be seen within the β (bcc) phase visible as bright in the

dark field image (DF1) taken using the $0\bar{1}\bar{1}\bar{1}$ reflection marked in SADP1. The dark particle with parallel boundaries without precipitates is also visible. The SADP2 taken of this phase was identified as the α phase of [12 $\bar{3}$ 1] zone axis. Two types of the α (hcp) phase exist: (i) primary large particles present already after quenching and (ii) fine precipitates formed during ageing at 200 °C. The precipitates are responsible for strengthening of the alloy after ageing. Fig. 15a shows the STEM micrograph and elemental mapping (Fig. 15a and b) taken of the alloy 2 aged 10 minutes to the maximum hardness at 200 °C. The elongated precipitates of length about 70 nm can be seen and similarly like in Fig. 12 they reveal enrichment in scandium, however the depletion in magnesium is not clear. Most probably the precipitates rich in scandium cause additional lattice stresses and as result, quite significant precipitation strengthening is obtained. Fig. 16 derives the HRTEM micrograph of alloy 2 aged to the maximum hardness at 200 °C. The Fast Fourier Transform FFT images (inserted in Fig. 16) from the areas marked by white squares showing the symmetry analogical to [01 $\bar{1}$ 0] α (hcp) phase and [001] β (bcc) phase. These results confirm the electron diffraction

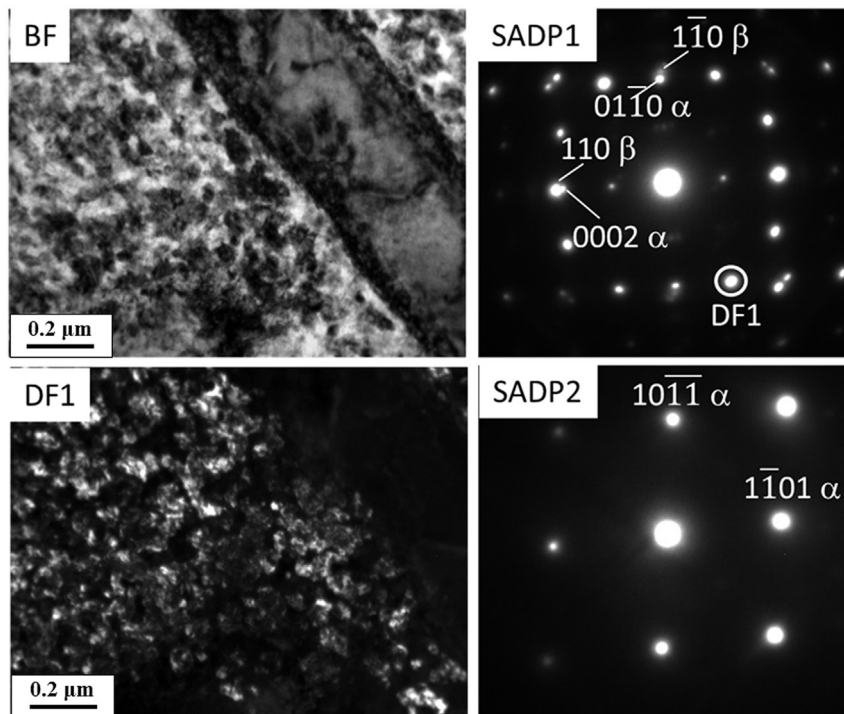


Fig. 14. TEM bright field and dark field micrographs of Mg9Li6Sc quenched from 520 °C/1.5h and aged at 200 °C for 10 minutes to maximum hardness. SADP1 taken of β (bcc) phase on the left and SADP2 of the dark elongated grain on the right. DF taken using $0\bar{1}\bar{1}\bar{1}$ reflection marked in SADP as DF1.

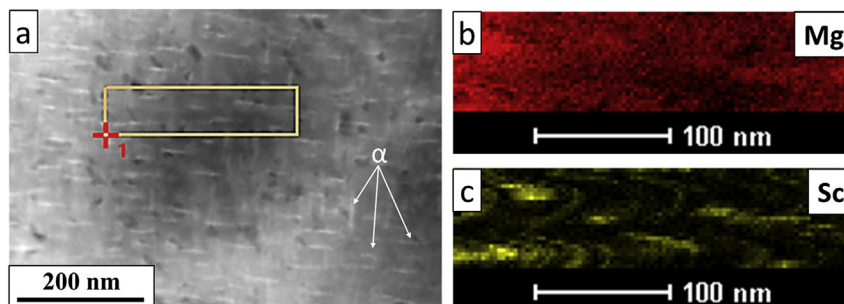


Fig. 15. a) STEM micrograph and elemental mapping distribution b) Mg, c) Sc, taken from alloy Mg9Li6Sc quenched from 520 °C/1.5h and aged for 10 minutes at 200 °C showing distribution of magnesium and scandium within the large particle.

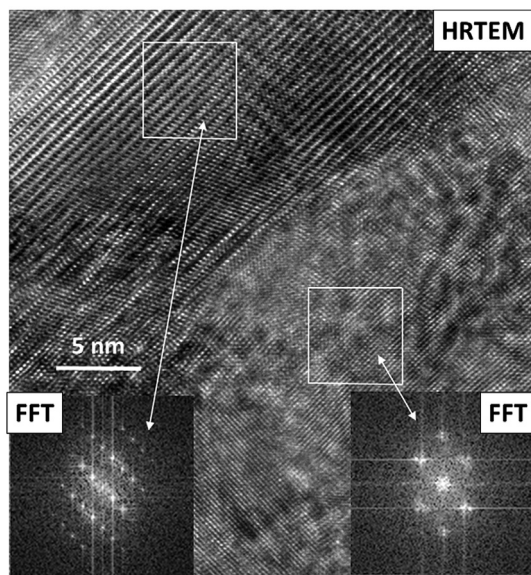


Fig. 16. HRTEM from alloy Mg9Li6Sc aged to maximum hardness at 200 °C/10min after quenching from 520 °C/1/5h showing α (hcp) precipitate within β (bcc) matrix as results from FFT images taken of marked areas.

interpretation in Figs. 13 and 14 indicating the precipitation of α (hcp) phase at [01 $\bar{1}$ 0] zone axis orientation within the β (bcc) matrix of [001] zone axis orientation. One can see double space (0001) α (hcp) planes parallel to the (110) β (bcc) ones. Frequent dislocations (marked by arrows in densely packed planes can be seen formed due to interface matching. In addition, a high density of crystal defects particularly within the α (hcp) phase points to a high level of stresses at the interface contributing to the increase of hardness after ageing. The densely packed {110} β (bcc) planes parallel to densely packed {0001} planes of the α (hcp) phase found already in conventional SADP were confirmed by the HRTEM.

4. Conclusions

1. The ternary Li-Mg-Sc phase diagram has been extrapolated (up to 20 wt.% of Li and Sc) from the binary systems under assumption that the phases with the same crystallographic structure have the same models. The results show that, the β (bcc) solid solution crystallizes as a primary phase and the scandium addition increases the range of primary crystallization of the β (bcc) phase similarly to Mg9Li alloy. The phase diagram calculation indicates that in the alloy containing 9% Li and only 3% Sc the β (bcc) phase crystallizes first. The computed isothermal section at 400 °C suggests that the Mg9Li3Sc alloy should consist only of the β (bcc) phase at 400 °C, while the alloy with 9% Li and 6% Sc at 400 °C should comprise the β (bcc) + MgSc phases.
2. The Mg9Li base alloys containing 3 and 6 wt.% Sc after quenching from temperatures above 400 °C are constituted of grains of β (bcc) phase with the particles of MgSc phase as identified using the electron diffraction technique. It indicates that the β (bcc)/ β (bcc) + MgSc phase boundary in the calculated phase diagram should be shifted toward lower scandium contents.
3. The investigated alloys containing Sc revealed precipitation hardening during ageing at 160 and 200 °C causing the hardness increase from 74 to 93 HV after 40 minutes at 160 °C for the alloy with 6% Sc. The precipitates of size below 100 nm were identified as the α Mg solid solution rich in scandium. EDS imaging

indicated increased scandium content within the precipitates which contributed to a high stress level at the α (hcp)/ β (bcc) interface manifested by a high dislocation density particularly within the α (hcp) phase.

Acknowledgements

The financial support of the National Science Centre Poland (NCN) under project OPUS number 2014/15/B/ST8/03184 is gratefully acknowledged.

References

- [1] B.L. Mordike, T. Ebert, Magnesium. Properties — applications — potential, *Mater. Sci. Eng. A* 302 (2001) 37–45.
- [2] S. Karewar, N. Gupta, S. Groh, E. Martinez, A. Caro, S.G. Srinivasan, Effect of Li on the deformation mechanisms of nanocrystalline hexagonal close packed magnesium, *Comput. Mater. Sci.* 126 (2017) 252–264.
- [3] Y. Ogawa, D. Ando, Y. Sutou, J. Koike, A lightweight shape-memory magnesium alloy, *Science* 353 (2016) 368–370.
- [4] I.J. Polmear, Review on research and development of magnesium, *Alloy Mater. Sci. Technol.* 10 (1994) 1–15.
- [5] Z. Yang, J.P. Li, J.X. Zhang, G.W. Lorimer, J. Robson, Review on research and development of magnesium, *Acta Metall. Sin. (Engl. Lett.)* 21 (2008) 313–328.
- [6] D. Xu, E.-h. Han, Y. Xu, Effect of long-period stacking ordered phase on microstructure, mechanical property and corrosion resistance of Mg alloys: a review, *Prog. Nat. Sci. Mater. Int.* 26 (2016) 117–128.
- [7] J. Gao, Y. Chen, Y. Wang, Effect of Sn element on the formation of LPSO phase and mechanical properties of Mg-6Y-2Zn alloy, *Mater. Sci. Eng. A* 711 (2018) 334–342.
- [8] S. Pathak, N. Velisavljevic, J.K. Baldwin, M. Jain, S. Zheng, M. Nathan, A. Beyerlein, J. Strong, Ductile, and thermally stable bcc-Mg nanolaminates, *Sci. Rep.* 7/1 (2017).
- [9] M. Furui, Ch. Xu, T. Aida, M. Inoue, H. Anada, T.G. Langdon, Improving the superplastic properties of a two-phase Mg-8% Li alloy through processing by ECAP, *Mater. Sci. Eng. A* 410–411 (2005) 439–442.
- [10] J. Dutkiewicz, Ł. Rogal, P. Fima, P. Ozga, Composites strengthened with graphene platelets and formed in semisolid state based on α and α/β MgLiAl alloys, *J. Mater. Eng. Perform.* 27 (2018) 2205–2215.
- [11] X. Liu, R. Wu Z. Niu, J. Zhang, M. Zhang, Superplasticity at elevated temperature of an Mg-8%Li-2%Zn alloy, *J. Alloys Compd.* 541 (2012) 372–375.
- [12] W.J. Kim, M.J. Kim, J.Y. Wang, Ultrafine-grained Mg-9Li-1Zn alloy sheets exhibiting low temperature superplasticity, *Mater. Sci. Eng. A* 516 (2009) 17–22.
- [13] G.H. Park, J.T. Kim, H.J. Park, Y.S. Kim, H.J. Jeong, N. Lee, Y. Seo, J.-Y. Suh, H.-T. Son, W.-M. Wang, J.M. Park, K.B. Kim, Development of lightweight Mg-Li-Al alloys with high specific strength, *J. Alloys Compd.* 680 (2016) 116–120.
- [14] H.P. Yang, M.W. Fu, S. To, G.C. Wang, Investigation on the maximum strain rate sensitivity (m) superplastic deformation of Mg-Li based alloy, *Mater. Des.* 112 (2016) 151–159.
- [15] G. Sha, X. Sun, T. Liu, Y. Zhu, T. Yu, Effects of Sc addition and annealing treatment on the microstructure and mechanical properties of the as-rolled Mg-3Li alloy, *J. Mater. Sci. Technol.* 27/8 (2011) 753–758.
- [16] C.J. Silva, A. Kula, R.K. Mishra, M. Niewczasz, Mechanical properties of Mg-Sc binary alloys under compression, *Mater. Sci. Eng. A* 692 (2017) 199–213.
- [17] Y. Ogawa, D. Ando, Y. Sutou, K. Yoshimi, J. Koike, Determination of α/β phase boundaries and mechanical characterization of Mg-Sc binary alloys, *J. Alloys Compd.* 670 (2016) 335–341.
- [18] Y. Ogawa, Y. Sutou, D. Ando, J. Koike, Aging precipitation kinetics of Mg-Sc alloy with bcc-hcp two-phase, *Mater. Sci. Eng. A* 670 (2016) 335–341.
- [19] D. Ando, Y. Ogawa, T. Suzuki, Y. Sutou, J. Koike, Age-hardening effect by phase transformation of high Sc containing Mg alloy, *Mater. Lett.* 161 (2015) 5–8.
- [20] N. Saunders, A review and thermodynamic assessment of the Al-Mg and Mg-Li systems, *Calphad* 14 (1990) 61–70.
- [21] M.J. Bu, Y.B. Peng, M. Wang, et al., Thermodynamic optimization of the Sc-X (X = La, Li, Ca, Cr) systems, *J. Phase Equilib. Diffus.* 33 (2012) 40–45.
- [22] A. Pisch, R. Schmid-Fetzer, G. Cacciamani, P. Riani, A. Saccone, R. Ferro, Mg-rich phase equilibria and thermodynamic assessment of the Mg-Sc system, *Z. Metallkde* 89 (1998) 474–477.
- [23] Y.-B. Kang, A.D. Pelton, P. Chartrand, C.D. Fuerst, Critical evaluation and thermodynamic optimization of the Al-Ce, Al-Y, Al-Sc and Mg-Sc binary systems, *Calphad* 32 (2008) 413–422.
- [24] H. Okamoto, Li-Sc (Lithium-Scandium), *J. Phase Equilib. Diffus.* 30 (2009) 117.
- [25] N.N. Ganiev, Kh.M. Nazarov, M.D. Badalov, Interaction of lithium with rare-earth metals, *Izv. Ross. Akad. Nauk. Metall.* 6 (1998) 109–112.
- [26] H.L. Lukas, S.G. Fries, B. Sundman, *Computational Thermodynamics: the Calphad Method*, Cambridge University Press, Cambridge, UK, 2007.
- [27] J. Dutkiewicz, S. Ruzs, D. Kuc, O. Hilsner, P. Paika, G. Boczkaj, Superplastic deformation of two phase MgLiAl alloy after TCAP pressing, *Acta Metal. Slov.* 23 (2017) 215–221.

- [28] Y. Zou, L. Zhang, H. Wang, X. Tong, M. Zhang, Z. Zhang, Texture evolution and their effects on the mechanical properties of duplex Mg-Li alloy, *J. Alloys Compd.* 669 (2016) 72–78.
- [29] U.R. Kattner, W.J. Boettinger, On the Sn-Bi-Ag ternary phase diagram, *J. Electron. Mater.* 23 (1994) 603–610.
- [30] R. Schmid-Fetzer, J. Grobner, Thermodynamic database for Mg alloys - progress in multicomponent modeling, *Metals* 2 (2012) 377–398.
- [31] Y. Ogawa, D. Ando, Y. Sutou, J. Koike, Aging effect of Mg-Sc alloy with $\alpha+\beta$ two-phase microstructure, *J. Jpn. Inst. Met. Mater.* 80 (3) (2016) 171–175.
- [32] Ch-W. Yang, T.-S. Lui, L.-H. Chen, H.-E. Hung, Tensile mechanical properties and failure behaviors with the ductile to-brittle transition of the $\alpha+\beta$ type Mg-Li-Al-Zn alloy, *Scripta Mater.* 61 (2009) 1141–1144.
- [33] T. Liu, S.D. Wu, S.X. Li, P.J. Li, Microstructure evolution of Mg-14% Li-1% Al alloy during the process of equal channel angular pressing, *Mater. Sci. Eng. A* 460–461 (2007) 499–503.
- [34] L.L. Rokhlin, Magnesium alloys containing rare earth metals: structure and properties, in: J.N. Fridlyander, G.G. Eskin (Eds.), *Advances in Metallic Alloys*, 2003, pp. 34–68.

Jan Dutkiewicz*, Łukasz Rogal**, Damian Kalita, Przemysław Fima
Institute of Metallurgy and Materials Science of the Polish Academy of Sciences, Reymonta 25 Str., Krakow Poland

* Corresponding author.

** Corresponding author.

E-mail addresses: j.dutkiewicz@imim.pl (J. Dutkiewicz),
l.rogal@imim.pl (Ł. Rogal).

31 August 2018

13 December 2018

Available online 19 December 2018